Published in final edited form as:
Science. 2009 May 8; 324(5928): 804–807. doi:10.1126/science.1168683.

Mammalian expression of infrared fluorescent proteins engineered from a bacterial phytochrome

Xiaokun Shu[1,2], **Antoine Royant**[3], **Michael Z. Lin**[2], **Todd A. Aguilera**[2], **Varda Lev-Ram**[2], **Paul A. Steinbach**[1,2], and **Roger Y. Tsien**[1,2,4,*]

[1]Howard Hughes Medical Institute, University of California at San Diego, 9500 Gilman Drive, La Jolla, California 92093-0647, USA

[2]Department of Pharmacology, University of California at San Diego, 9500 Gilman Drive, La Jolla, California 92093-0647, USA

[3]Institut de Biologie Structurale UMR 5075 CNRS-CEA-UJF, 41, rue Jules Horowitz, 38027 Grenoble CEDEX 1, France

[4]Department of Chemistry and Biochemistry, University of California at San Diego, 9500 Gilman Drive, La Jolla, California 92093-0647, USA

Abstract

Visibly fluorescent proteins (FPs) from jellyfish and corals have revolutionized many areas of molecular and cell biology, but the use of FPs in intact animals such as mice has been handicapped by poor penetration of excitation light. We now show that a bacteriophytochrome from *Deinococcus radiodurans* incorporating biliverdin as the chromophore can be engineered into monomeric, infrared-fluorescent proteins (IFPs), with excitation/emission maxima of 684/708 nm respectively, extinction coefficient > 90,000 $M^{-1}cm^{-1}$, and quantum yield 0.07. IFPs express well in mammalian cells and mice, and spontaneously incorporate biliverdin, which is ubiquitous as the initial intermediate in heme catabolism but has negligible fluorescence by itself. Because their wavelengths penetrate tissue well, IFPs are suitable for whole-body imaging. The IFPs developed here provide a scaffold for further engineering.

In vivo optical imaging of deep tissues in animals is most feasible between 650 and 900 nm because such wavelengths minimize the absorbance by hemoglobin, water and lipids as well as light scattering (1,2). Thus, genetically encoded infrared fluorescent proteins would be particularly valuable for whole-body imaging in cancer and stem cell biology (3,4), gene therapy etc. However, excitation and emission maxima of FPs have not yet exceeded 598 and 655 nm respectively (5–7). Somewhat longer wavelengths (644 nm excitation, 672 nm emission) have been observed in a phytochrome-based FP that incorporates phycocyanobilin (PCB) as the chromophore (8). However, neither incorporation of exogenous phycocyanobilin nor transfer of its biosynthetic pathway into animal cells has yet been demonstrated. Bacterial phytochromes are more promising because they incorporate biliverdin IXα (BV) instead of PCB (9), and BV is the initial intermediate in heme catabolism by heme oxygenase in all aerobic

*To whom correspondence should be addressed. E-mail: rtsien@ucsd.edu.

Supporting Online Material
www.sciencemag.org
Materials and Methods
SOM Text
Figs. S1 to S11
Table S1

organisms including animals. For example, normal adult humans endogenously generate and metabolize 300 – 500 mg BV each day simply from routine heme breakdown (10). Recently, a full-length bacteriophytochrome (*Dr*BphP) from *Deinococcus radiodurans* with a single mutation (D207H) was reported to be red fluorescent at 622 nm upon excitation of the Soret band near 416 nm (11). Excitation of the Q band absorbing at 699 nm gave no fluorescence (11), contradicting Kasha's rule that fluorescence occurs from the lowest excited state. Emission peaks at 710–725 nm have been observed from various forms of *Rhodopseudomonas palustris* (12) and *Pseudomonas aeruginosa* (13) bacteriophytochromes expressed in *E. coli*, but fluorescence efficiencies have not been quantified and reconstitution in nonbacterial systems has not yet been demonstrated.

To minimize the probability of nonradiative decay, we chose to limit *Dr*BphP to its chromophore-binding domain (CBD), consisting of the PAS and GAF domains, which are necessary and sufficient for covalent incorporation of BV (14,15). We discarded the PHY domain and the C-terminal histidine kinase related domain (HKRD) (9), which transduce excited state energy into conformational change and biochemical signaling (15). A gene encoding *Dr*CBD (321 amino acids) with the D207H mutation was synthesized with codons optimized for *Escherichia coli* (16). When coexpressed with cyanobacterial heme oxygenase (HO-1) in *E. coli* and excited near 700 nm, the truncated mutant fluoresced in the infrared with emission maximum of 722 nm. However, this mutant, dubbed IFP1.0, is weakly fluorescent (Table S1), reversibly photofatiguable (Fig. S1), and dimeric (Fig. S2). The dimerization of IFP1.0 is due to at least 4 residues (Y307/L311/L314/V318) through hydrophobic interactions (Fig. S3A).

Based on the crystal structure of *Dr*CBD (15), nonradiative decay of the excited chromophore is probably promoted by rotation of the D pyrrole ring due to relatively sparse packing of surrounding residues. Multiple sequence alignment of >100 phytochromes revealed conserved residues, some of which may contribute to photoisomerization [see supporting online material (SOM) text]. In order to increase the brightness of IFP1.0, 14 residues near the D ring were chosen and divided into 7 groups for saturation mutagenesis (Fig. 1A), followed by DNA shuffling, which generated IFP1.1, with excitation and emission maxima of 686 and 713 nm, respectively, and about 2.6 fold greater brightness than IFP1.0 (Table S1). Several more rounds of directed evolution of IFP1.1 led to IFP1.4 (Fig. S4).

IFP1.4 is ~ 4 times brighter than IFP1.0 (Table S1) and its fluorescence is stable over a wide pH range from 5 to 9 (Fig. S5). IFP1.4 is monomeric (Fig. S2) and no longer shows significant reversible photofatigue (Fig. S1). At an excitation rate that initially produces 1000 emitted photons/s per molecule of IFP1.1 or 1.4, the time to photobleach by 50% ($t_{1/2}$) is 8.5 or 8.4 s respectively. For comparison, $t_{1/2}$ of the popular yellow fluorescent protein "Venus" is 15 s (17). A rationally introduced mutation L311K replaced a hydrophobic group by a charged amino acid and disrupted the dimer interface in IFP1.2 (Fig. S3B). Mutation A288V likely eliminated the residual photoconversion of IFP1.0 since two additional methyl groups of Val288 may limit the D ring rotation. However, the excitation and emission maxima of IFP1.4, 684 and 708 nm respectively, are slightly blue shifted compared to IFP1.0 (Fig. 1B). The blue shift may have resulted from using 676 nm excitation, the longest-wavelength laser line available to us, to select for higher brightness during fluorescence activated cell sorting (FACS).

Expression of IFP1.4 alone without exogenous BV leads to bright and homogeneous infrared fluorescence in human embryonic kidney cells (HEK293A) (Fig. 2A). Furthermore, exogenously added BV further increases infrared fluorescence of transfected cells including neurons (Fig. S6), proving that BV is membrane-permeant and adds rapidly to fill IFP1.4 when

endogenous BV had not saturated the protein. The half-life of IFP1.4 is about 4 hours in HEK293A cells (Fig. S7, Fig S8).

As a simple demonstration that IFP1.4 fusions can be functional, IFP1.4 was fused to the pleckstrin homology (PH) domain of human AKT1 (18). This PH domain is known to bind to phosphatidylinositol-3,4,5-trisphosphate formed at the plasma membrane after growth factor stimulation. Serum-starved HEK293 cells expressing the IFP1.4-PH^{AKT1} fusion showed IR fluorescence diffusely distributed in the cytosol, but this signal translocated to the plasma membrane within 10 min after insulin stimulation (Fig. 2B), illustrating that IFP1.4 can image the trafficking of fusion proteins.

Expression of IFPs in intact mice via adenovirus serotype 5 (Ad5) also produced infrared fluorescence. Ad5 is well known to infect mouse liver specifically (19). Two modified Ad5 were generated: Ad5I and Ad5K. Ad5I contains the genes for IFP1.1 and GFP, the latter controlled by an internal ribosome entry sequence (IRES) (16). Ad5K encodes mKate, a red fluorescent protein advocated for *in vivo* imaging (5), and IRESGFP. Weak infrared fluorescence of liver was detected 5 days after intravenous (IV) injection of Ad5I through tail vein (Fig. 3A). The whole liver was easily detected after IV injection of 250 nmole (~7 mg/kg) BV (Fig. 3A). The increase in liver fluorescence was half-maximal in ~10 min and maximal (~ 5-fold) 1 hour after BV injection (Fig. 3B). Resolution of IFP fluorescence from background autofluorescence can be enhanced by spectral deconvolution (Fig. 3C). The three-dimensional distribution of IFP fluorescence in the mouse liver can be reconstructed tomographically (Fig. S9). BV injection did not cause observable toxicity in mice (20). Furthermore, higher doses of BV (35–50 mg/kg) have been reported to give beneficial protection *in vivo* against reactive oxygen species (21) and transplantation-induced injury (22). As a control, IV injection of 250 nmole BV did not generate infrared fluorescence in either Ad5K infected (Fig. 3A) or non-virus infected mice (data not shown). The far-red fluorescence of mKate was observed in Ad5K infected liver, and was unaffected by BV. Neither Ad5I nor Ad5K infected mice displayed GFP fluorescence in the liver of intact mice (Fig. 3A). Removal of the overlying skin, followed by complete exposure of the liver, increased the mKate fluorescence by a much greater factor than for the IFP signal (Fig. 4 and Fig. S10), illustrating how overlying tissues attenuate mKate's excitation and emission wavelengths to a greater extent than those for IFP.

The entire dissected liver was fluorescent for mice expressing IFP and mKate (Fig. S11), suggesting virus infection of the whole liver. GFP fluorescence became visible only after complete extraction of the liver and was similar for Ad5I vs. Ad5K (Fig. S11), suggesting similar efficiencies of viral infection. Fluorescence microscopy of frozen sections showed fluorescence increasing in the order IFP1.1 < mKate < GFP fluorescence (Fig. 4C), confirming that IFP remains detectable in histology and that its improved visibility *in vivo* is due not to higher expression levels but rather to superior penetration of longer excitation and emission wavelengths through bulk pigmented tissue.

IFPs can be imaged over spatial scales from subcellular resolution up to strongly pigmented organs within intact whole mammals, whereas luciferase-based bioluminescence is useful mainly for whole-body imaging (23). The wavelengths of IFPs are particularly well-suited to optical tomographic reconstruction (Fig. S9,24). Even for microscopic imaging where existing FPs are highly effective, IFPs should reduce the contribution of cellular autofluorescence, enable excitation by cheap laser diodes, add new wavelengths for multicolor labeling, and accept resonance energy transfer from other dyes, FPs, or bioluminescent proteins. BV is uniquely advantageous as a cofactor because it is spontaneously and irreversibly incorporated into bacteriophytochromes (25), nontoxic at appropriate doses (20–22), nonfluorescent by itself, endogenously produced, and can be further supplemented either by expression of heme oxygenase or by direct administration of commercially available material. Heme oxygenase is

an important enzyme in its own right and is involved in various diseases (26). Its cumulative activity could be monitored by IFP fluorescence if apoprotein expression were in excess over BV. More than 1500 bacteriophytochrome-like sequences are already available in the NCBI and CAMERA databases (27). These genes should provide raw material for selection and directed evolution of photochemical transducers based on a scaffold completely independent of the 11-stranded beta-barrel of coelenterate FPs.

Supplementary Material

Refer to Web version on PubMed Central for supplementary material.

References and Notes

1. Jöbsis FF. Science 1977;198:1264. [PubMed: 929199]
2. Weissleder R, Ntziachristos V. Nat. Med 2003;9:123. [PubMed: 12514725]
3. Schroeder T. Nature 2008;453:345. [PubMed: 18480816]
4. Weissleder R, Pittet MJ. Nature 2008;452:580. [PubMed: 18385732]
5. Shcherbo D, et al. Nat. Methods 2007;4:741. [PubMed: 17721542]
6. Shkrob MA, et al. Biochem. J 2005;392:649. [PubMed: 16164420]
7. Wang L, Jackson WC, Steinbach PA, Tsien RY. Proc. Natl. Acad. Sci. U.S.A 2004;101:16745. [PubMed: 15556995]
8. Fischer AJ, Lagarias JC. Proc. Natl. Acad. Sci. U.S.A 2004;101:17334. [PubMed: 15548612]
9. Davis SJ, Vener AV, Vierstra RD. Science 1999;286:2517. [PubMed: 10617469]
10. Harris, JW.; Kellermeyer, RW. The Red Cell. Cambridge, Massachusetts: Harvard Univ. Press; 1970.
11. Wagner JR, et al. J. Biol. Chem 2008;283:12212. [PubMed: 18192276]
12. Giraud E, et al. J. Biol. Chem 2005;280:32389. [PubMed: 16009707]
13. Yang X, Kuk J, Moffat K. Proc. Natl. Acad. Sci. U.S.A 2008;105:14715. [PubMed: 18799746]
14. Rockwell NC, Su YS, Lagarias JC. Annu. Rev. Plant Biol 2006;57:837. [PubMed: 16669784]
15. Wagner JR, Brunzelle JS, Forest KT, Vierstra RD. Nature 2005;438:325. [PubMed: 16292304]
16. Materials and methods are available as supporting material on *Science* Online.
17. Shaner NC, Steinbach PA, Tsien RY. Nat. Methods 2005;2:905. [PubMed: 16299475]
18. Bellacosa A, Testa JR, Staal SP, Tsichlis PN. Science 1991;254:274. [PubMed: 1833819]
19. Waddington SN, et al. Cell 2008;132:397. [PubMed: 18267072]
20. 6 mice after BV injection were observed for 3 days (the maximum time that we could hold mice for imaging according to our university approved animal protocol).
21. Ollinger R, et al. Antioxid. Redox. Signal 2007;9:2175. [PubMed: 17919067]
22. Atsunori N, et al. Gastroenterology 2004;127:595. [PubMed: 15300591]
23. Contag CH, Bachmann MH. Annu. Rev. Biomed. Eng 2002;4:235. [PubMed: 12117758]
24. Ntziachristos V, et al. Proc. Natl. Acad. Sci. U.S.A 2004;101:12294. [PubMed: 15304657]
25. Electrospray mass spectrometry of bacterially expressed IFP1.4 holoprotein in 5% acetonitrile, 0.05% trifluoroacetic acid reported an average molecular weight (MW) of 36,342 Da, within experimental error of the MW (36,332 Da) expected from covalent incorporation of BV (582.6 Da) into the apoprotein (35,749.6 Da) from Ala2 to the C-terminus.
26. Abraham NG, Kappas A. Pharmacol. Rev 2008;60:79. [PubMed: 18323402]
27. Rusch DB, et al. PLoS Biol 2007;5:e77. [PubMed: 17355176]

28. We thank Drs. J. Clark Lagarias and Seth Field for donation of cDNAs encoding HO-1 and AKT1's PH domain respectively; John M. Saathoff and Geraldine Tran for help with plasmid purification; Margaret Timmers for help with tissue culture; Dr. Stephen Adams for help with light scattering measurements; Dr. Larry Gross for mass spectrometry; and Qing Xiong for flow cytometry. This work was supported by NIGMS grant R01 GM086197 and the Howard Hughes Medical Institute.

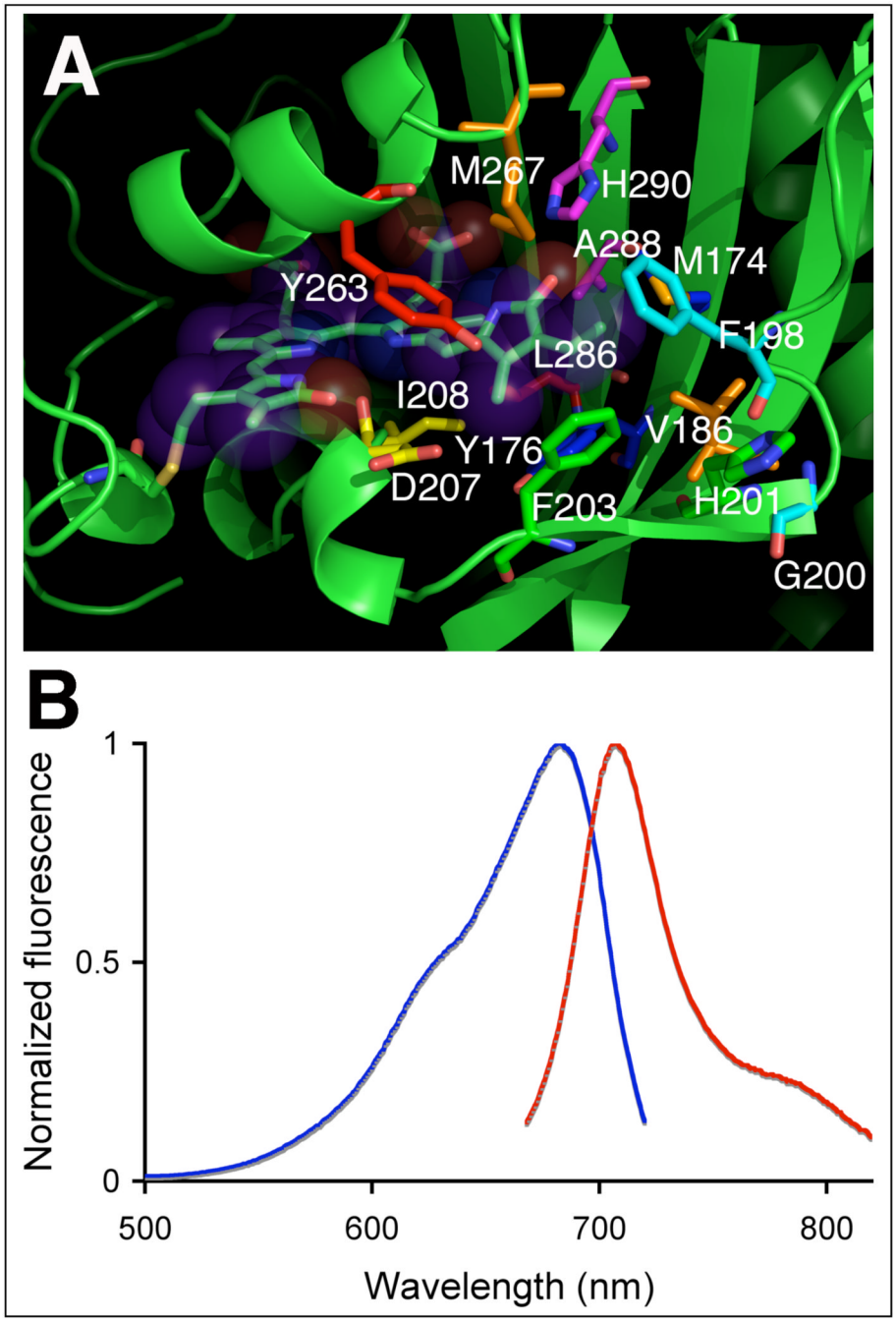

Fig. 1.

Infrared fluorescent proteins created by structure-based engineering of a bacteriophytochrome. (**A**) 14 residues surrounding the biliverdin (violet) in *Dr*CBD (PDB ID: 1ztu) (14) were divided into 7 groups (shown in different colors) and targeted for mutagenesis. (**B**) Normalized excitation (blue) and emission (red) spectra of IFP1.4.

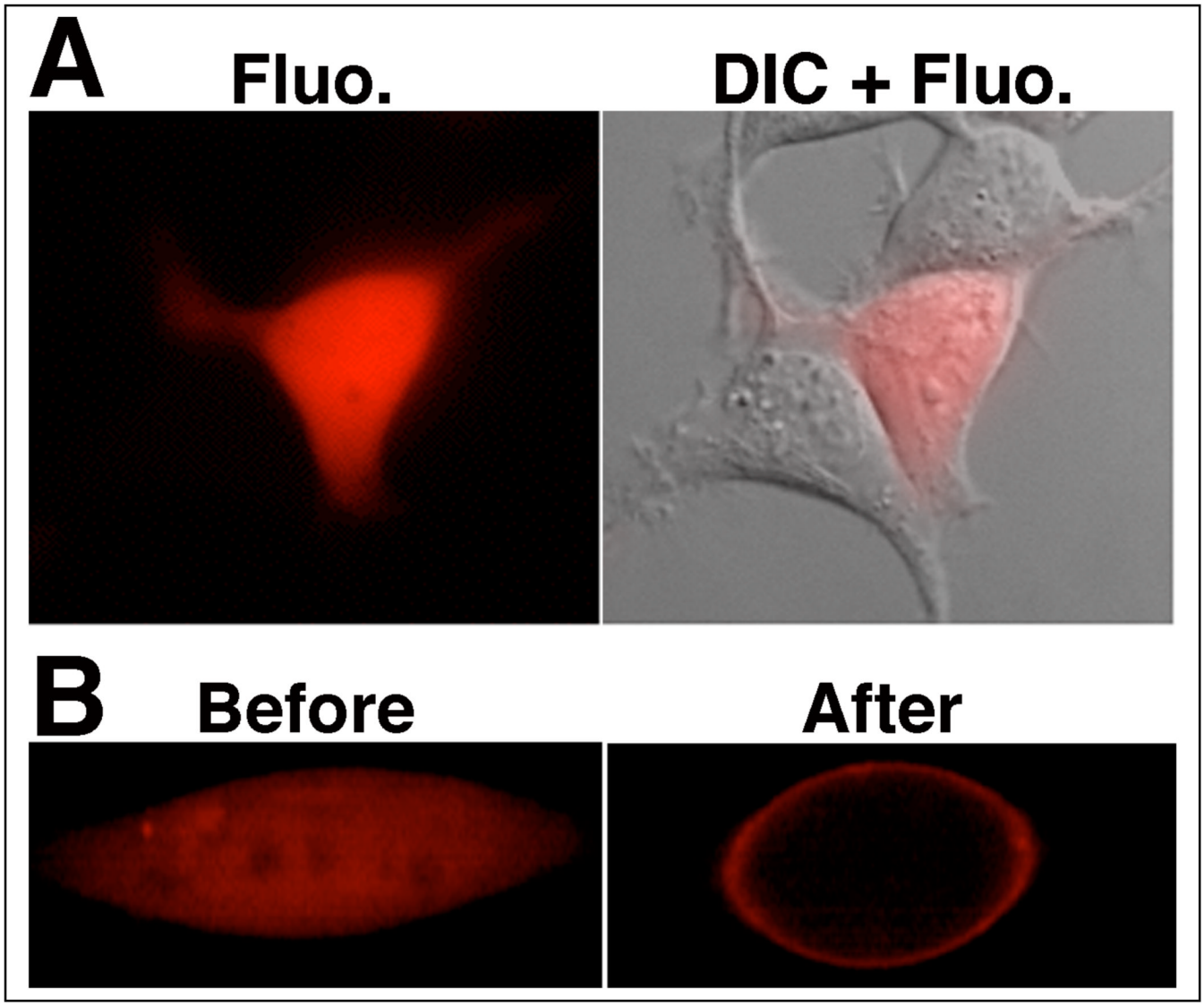

Fig. 2.

Imaging of IFP1.4 and IFP1.4-PH^{AKT1} in HEK293A cells. (**A**) Fluorescence image of IFP1.4 taken with Cy5.5 filter set (665 ± 22.5 nm excitation, 725 ± 25 nm emission). (**B**) Confocal laser-scanning microscopy of IFP1.4-PH^{AKT1} before and after insulin stimulation (excitation by 635 nm laser, emission by 650 nm long pass filter).

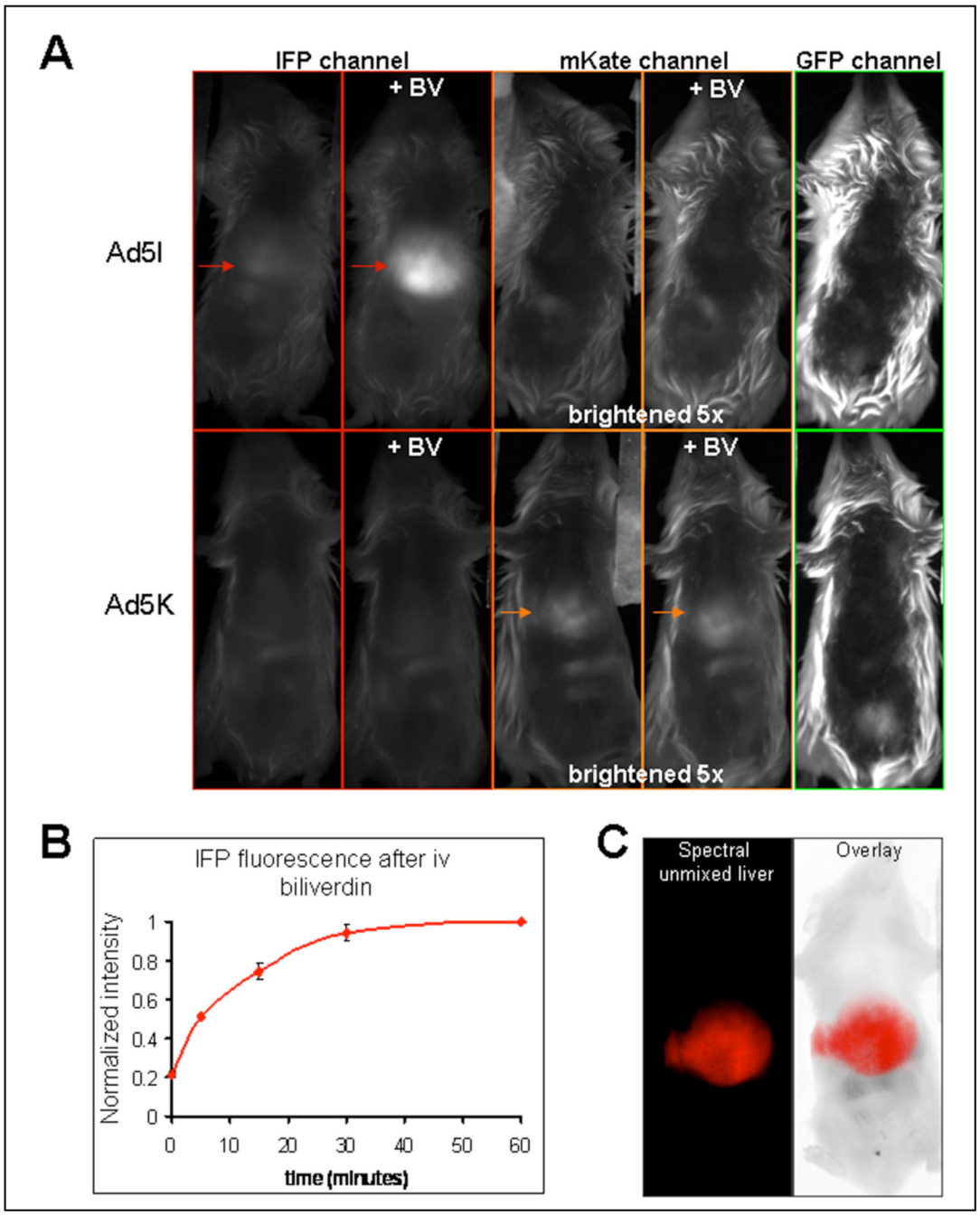

Fig. 3.

Imaging of GFP, mKate, and IFP1.1 in living mice. (**A**) Liver fluorescence of living mice injected with Ad5I (top row) and Ad5K (bottom row), imaged in the IFP excitation/emission channel before and after BV administration, mKate channel before and after BV, and GFP channel (14). Images through the mKate channel have been 5X brightened in software to render them visible, so the relative gains of the IFP channel, mKate channel, and GFP channel were 1, 5, and 1 respectively. The labeling above the images indicates the fluorescence channel. Arrows point to the liver. Note that the GFP images are dominated by autofluorescence, rendering the livers invisible. (**B**) Time course of averaged and normalized Ad5I liver fluorescence before and after BV injection. (**C**) Images of IFP-expressing mouse showing

spectrally deconvoluted liver fluorescence (left, red) and its overlay (right) with autofluorescence (grey).

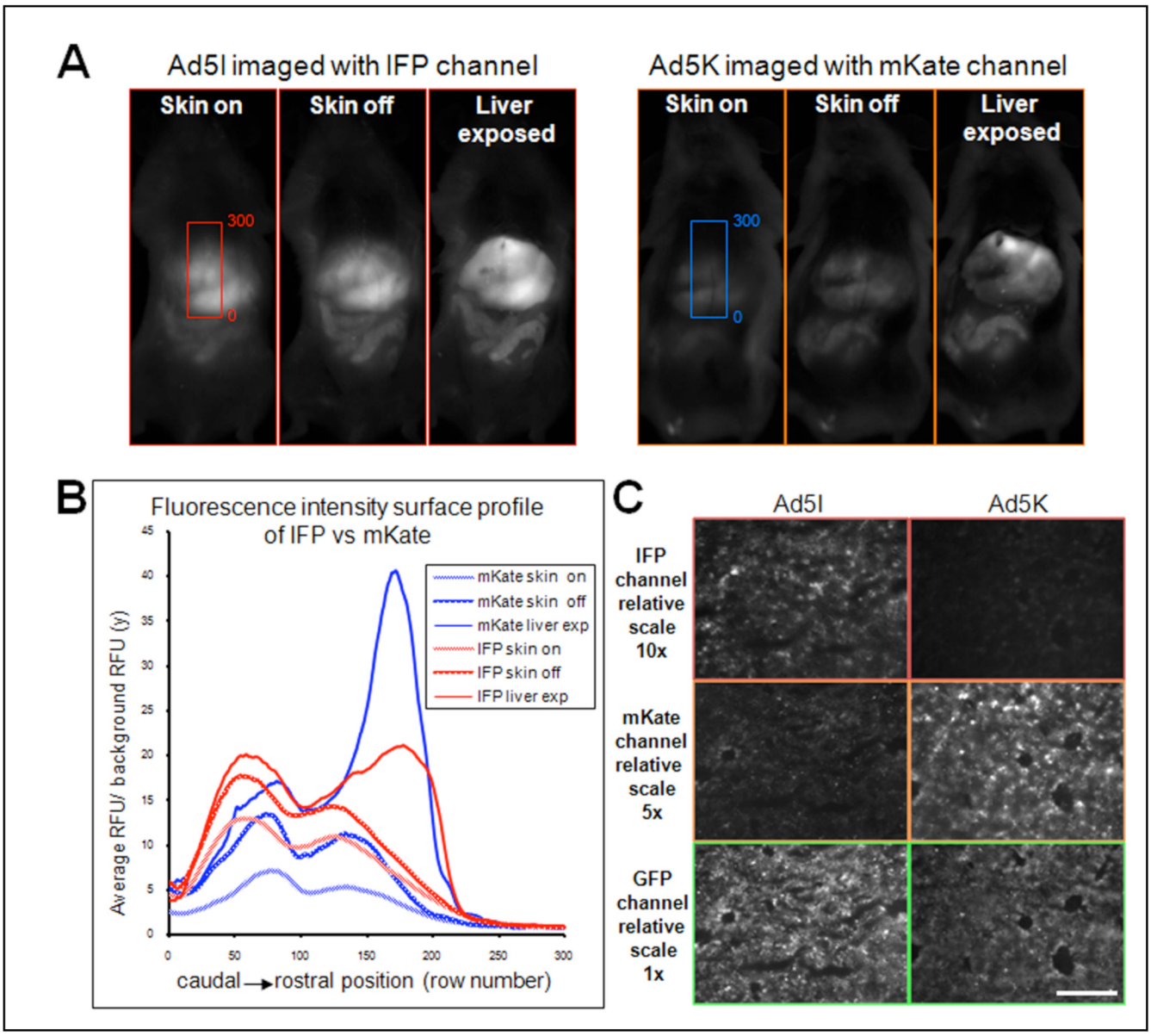

Fig. 4.

Analysis of mKate and IFP1.1 visibility and expression levels in livers of mice infected with Ad5I and Ad5K. (**A**) IFP/mKate fluorescence images before dissection (skin on), after removal of skin (skin off), and after removal of overlying peritoneum and ribcage (liver exposed). mKate images were 2.5X brightened relative to IFP images. Note that Ad5I infected mouse was imaged after 250 nmole IV injection of BV. See bright field images in Fig. S9. (**B**) Fluorescence intensity (signal over noise ratio) analysis of livers from (A). Average of 80 pixels in the horizontal x axis divided by the average of the 30 most rostral horizontal lines from each of the images starting below the liver (i.e. signal/noise ratio), moving rostrally for 300 lines. (**C**) Frozen sections were imaged to show IFP, mKate and GFP expression using a fluorescence stereomicroscope (Lumar, Zeiss) (14), displayed with relative intensity gains of 10, 5, and 1 respectively. Scale bar is 200 μm.